

Development of Quantitative Tools for Assessment of Cerebellar Dysfunction

by

Aditi Garg

B.S., Massachusetts Institute of Technology (2003)

Submitted to the Department of Electrical Engineering and Computer
Science

in partial fulfillment of the requirements for the degree of

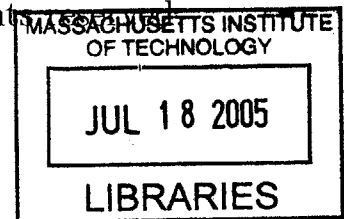
Master of Engineering in Electrical Engineering and Computer Science

at the

MASSACHUSETTS INSTITUTE OF TECHNOLOGY

January 2005 [February 2005]

© Massachusetts Institute of Technology 2005. All rights reserved.



Author

.....
Department of Electrical Engineering and Computer Science
January 7, 2005

Certified by.....

A handwritten signature in black ink, appearing to read "Steve G. Massaquoi".

.....
Steve G. Massaquoi
Assistant Professor
Thesis Supervisor

Accepted by ...

.....
Arthur C. Smith
Chairman, Department Committee on Graduate Students

BARKER

Development of Quantitative Tools for Assessment of Cerebellar Dysfunction

by

Aditi Garg

Submitted to the Department of Electrical Engineering and Computer Science
on January 7, 2005, in partial fulfillment of the
requirements for the degree of
Master of Engineering in Electrical Engineering and Computer Science

Abstract

Two tools for the quantitative assessment of cerebellar dysfunction are developed and explored. One is based on a battery of laptop tests designed for clinical use. Extensive analysis of one of the tests using a speed/accuracy trade-off shows a correlation of 0.74 with existing scoring systems. The second involves modeling the cerebellar function in arm movement as a PID controller. Initial results show trends toward asymmetry, higher values for Gk_{21} and Gk_{22} , and lower values for Gk_{11} and Gk_{12} as differences between the controller gains of ataxic subjects and control subjects when analyzing the trajectories of point to point movements. Further insight into these trends may lead to a deeper understanding of the cerebellum's function and dysfunction.

Thesis Supervisor: Steve G. Massaquoi
Title: Assistant Professor

Acknowledgments

Thank you to the people who have helped me learn this fascinating material.

Contents

1	Introduction	13
2	Background	15
2.1	Cerebellar Physiology and Anatomy	15
2.1.1	Basic Anatomy of the Cerebellum	16
2.1.2	Functions of the Cerebellum	16
3	Laptop based Assessment of Upper Limb and Finger Ataxia	19
3.1	Motivation	19
3.2	Design of Tests for the Laptop	20
3.3	Tests Developed	20
3.3.1	Time Keeper vs. Implementation System	20
3.3.2	Rhythmicity, Interdigit Coordination, and Single Limb Speed/Accuracy tradeoff	21
3.4	Software Design	23
3.5	Experimental Procedures	26
3.6	Results and Analysis	26
3.6.1	DL Testing	26
3.6.2	Tests a-d	30
4	Manipulandum and Model Based Assessment of Upper Limb Ataxia	35
4.1	Motivation and Strategy	35
4.2	Experimental Setup	36

4.3	Model	37
4.3.1	Model of Cerebral Interaction with Cerebellum	38
4.3.2	Cerebellum	39
4.3.3	Two Link Arm Model	39
4.3.4	Conversion from Joint to Cartesian Coordinates	43
4.3.5	Evaluating Fits of Trajectories	44
4.4	Experimental Subjects	44
4.5	Results	45
4.5.1	Fitting the Trajectories	46
5	Conclusions	53

List of Figures

2-1	Functional Relationships with the Cerebellum	16
3-1	Laptop Main Program Menu	23
3-2	Test Setup Window	24
3-3	Data Display Window	25
3-4	Average Time Interval for DL testing	27
3-5	Laptop Score, P_DL vs. MICARS Score	29
3-6	Laptop Score, P_DL vs. MICARS Arm Score	29
3-7	Z-Score Divisions	30
3-8	Internal Pacing Test	31
3-9	External Pacing Test	32
3-10	One Finger GH Test	33
3-11	Two Finger GH Test	34
4-1	Manipulandum Test Setup	36
4-2	Overview of RIPID Model	37
4-3	Diagram depicting Arm Model Parameters	40
4-4	Implementation of Two Link Arm Model	43
4-5	Sample Path Trajectories from a Control Subject	46
4-6	Sample Path Trajectories from a Patient Subject	46
4-7	Fitted Path Trajectory and Speed Profile of Subject P1 with Model	47
4-8	Fitted Path Trajectory and Speed Profile of Subject P2 and Model	48
4-9	Fitted Path Trajectory and Speed Profile of Subject C1 with Model	48
4-10	Fitted Path Trajectory and Speed Profile of Subject C2 with Model	49

4-11 Gb	50
4-12 Gk	50
4-13 I1	51

List of Tables

4.1	Subject Overview	44
4.2	Subject Parameters	45
4.3	Subject Arm Masses and Moments of Inertia	45
4.4	<i>R</i> squared values for Trajectory Fits	47

Chapter 1

Introduction

The cerebellum is a major part of the central nervous system that, among other things, appears to be involved in adaptively modulating spinal feedback needed for motor coordination. Disorders of the cerebellum can cause a person to have reduced coordination and accuracy (ataxia) during voluntary movements, and/or tremors.([3]) It is hoped that by studying subjects with functional as well as dysfunctional cerebellums, a further understanding of how the cerebellum modulates sensory feedback that assists in motor control and timing can be developed. This could possibly provide a basis for developing therapies for cerebellar disorders.

An easy and reliable method of quantitatively assessing patients can potentially provide a useful tool to better compare clinical cases and treatments. Creating a physiological model of the cerebellum and testing it against subject data will hopefully help in improving the understanding of how the cerebellum works.

Such understanding can help motivate new treatments. For example, if the normal processing of a signal for a movement is known, then in the scenario of a disease, it could potentially be artificially recreated to compensate for a malfunctioning cerebellum. This could then alleviate the symptoms and signs of ataxia.

Currently, a common practice in studying ataxia is to produce brain damage in experimental monkeys. Having an accurate model of a system allows one to simulate different conditions without having to use actual animals or humans.

The following describes the development of a continuously valued cerebellar as-

assessment tool to be administered on a laptop, as well as the analysis of point to point trajectories using an engineering model of the cerebellum with the purpose of furthering the quantitative assessment of how well the cerebellum works normally and fails in disease.

Chapter 2 describes the general background about the cerebellum's physiology.

Chapter 3 describes the development of the laptop assessment tool.

Chapter 4 describes the analysis of the point to point movement.

Chapter 5 contains the conclusions.

Chapter 2

Background

2.1 Cerebellar Physiology and Anatomy

The cerebellum is considered to be one of the seven major subdivisions of the central nervous system (CNS), the others being the spinal cord, medulla, pons, midbrain, diencephalon, and cerebral hemispheres. It is located in the caudal (towards the tail) section of the brain, dorsal to (towards the back of) the pons and the medulla, in the posterior region of the skull.

The cerebellum contains about half of the brain's neurons, which are arranged in a highly organized fashion, creating integrated circuit-like modules. About 40 times more axons project into the cerebellum than out of it. It receives inputs from the spinal cord, the cerebral cortex, and the vestibular organs of the inner ear, and provides circuits that project to the cerebral cortical and brain stem motor areas.([3]) This anatomy of the cerebellum is consistent with the hypothesis that the cerebellum receives feedback information from various sources and modulates the signals. Figure 2-1 shows a block diagram outlining these relationships. Thus damage or degeneration of the cerebellum leads to reduced control of movement and stability.

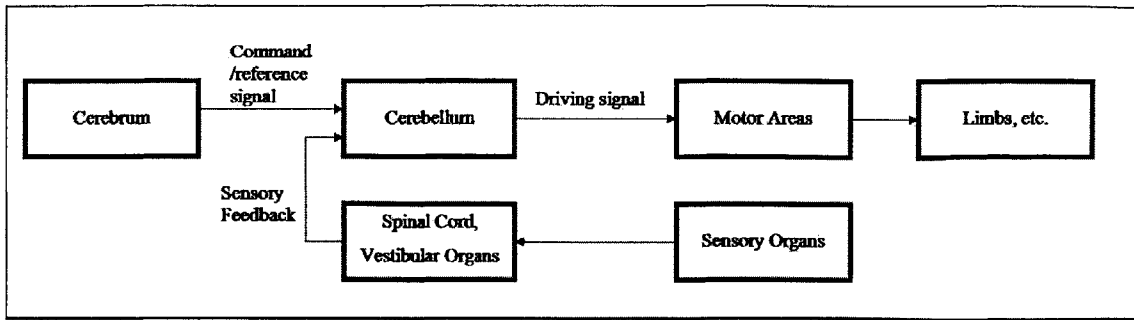


Figure 2-1: Functional Relationships with the Cerebellum

The cerebellum receives motor command signals from the cerebrum, and feedback signals from the spinal cord and vestibular organs from sensory organs such as muscle spindles. It is possible that the cerebellum modulates these signals before they reach the cerebral cortical and brain stem motor areas, which would result in the movements of the limbs, etc. Note that this diagram is a simplification of these relationships, and does not show all the connections between the various parts, but only the ones that have been focused on in the models that are explored in this thesis.

2.1.1 Basic Anatomy of the Cerebellum

The cerebellum has three major parts: the cerebrocerebellum (lateral cerebellum), the spinocerebellum (intermediate or medial cerebellum), and the vestibulocerebellum (flocculonodular lobe). The cerebellar cortex has 5 types of neurons, the inhibitory stellate, basket, Purkinje, Golgi, and excitatory granule cells. The axons of the granule cells run perpendicular to the Purkinje neurons, and are called parallel fibers. One of the two inputs to the cerebellar cortex is mossy fibers. They originate from nuclei in the spinal cord and brain stem, and carry sensory information to the granule cells.([3]) The second input is the climbing fibers that originate from the inferior olive of the brain, and wrap around the Purkinje neurons making synaptic contacts.([3], [6]) According to [6], the arrangement of these neurons may provide mechanisms for the gains of the circuit to be adjusted to provide adaptive feedback control that stabilizes and coordinates joint motion.

2.1.2 Functions of the Cerebellum

More recently, the cerebellum has been generally regarded as an adaptive controller.([6]) In general, a controller processes signals to optimize and enhance the performance of

the system, as well as provide stability. In this case, the cerebellum processes neural signals to provide smoothness, timeliness, recoverability, and accuracy to the system. In principle, when an action is performed, a controller can base its control exclusively on pre-stored or pre-formulated commands (feedforward control), or it can adjust its output commands on the basis of external information so that the desired result is obtained (feedback-dependent control). These two modes of control can coexist. According to some views, the commands are adjusted by amplifying or attenuating neural signals. The particular model explored here is based upon a model proposed in [7] which depicts the cerebellum as modulating tracking error signals (thus processing both feedforward and feedback information). If the controller (cerebellum) cannot adjust the neural signals properly, movements may overshoot targets, and trajectories may become jagged. The principal signs of cerebellar disease are ataxia, which refers to reduced coordination/control of movement, and tremor, which refers to instability in maintaining a posture. A major goal of quantitative assessment of function/dysfunction of the cerebellum is to measure the severity of ataxia and/or tremor. The quantitative measurement of ataxia is explored in this thesis.

Preliminary analysis in [7] suggests that ataxia is related to modified/reduced gains in cerebellar feedback, which would cause corrective action due to feedback to be weakened. If ataxia is due to reduced gains in cerebellar feedback, it may be hypothesized that ataxia can be characterized by decreased bandwidth for control. Fitts and Peterson ([1]) considered reduced bandwidth to mean that for any given speed of a point-to-point movement, there would be less accuracy (for example, a larger initial overshoot from a target). Conversely, for a given level of accuracy, there would be an increase in settling time. By this rationale, a subject with ataxia can achieve a given level of accuracy only by reducing the speed of movement relative to that of healthy subjects. Thus, ataxia corresponds to a less favorable speed accuracy trade-off for a given movement.

The cerebellum is also considered important for timing aspects of motor coordination as well as perception of time.([5]) In tests done by Keele and Ivry ([5]), subjects were asked to tap along with a pacing tone of 50 ms given every 550 msec. Once the

tapping of the subjects was synchronized with the tones, the pacing was terminated, and the subjects were asked to continue tapping 30 times after the pacing tone had been terminated. Subjects with cerebellar atrophy had a higher standard deviation of the interval times between taps than the control group. Tests on perception of time between intervals of tones that were multiples of 440 msec apart and perceiving the speed of a moving object were also done, as subjects with cerebellar damage have difficulty tracking moving objects with their eyes. ([5, p.187-88, 193-94])

Further analysis of the tapping test was done in accordance with a model developed by Wing and Kristofferson, in which there is a timekeeper or clock system and an implementation system that regulate periodic behavior. ([2, p. 149]) If the timekeeper system is intact, then if the tap is delayed relative to the pacing tone, then the next tap is quickened to compensate for it. However, if the response is delayed and there is no correction for it in the next clock cycle, it is taken to indicate that the implementation system is intact, but the timekeeper system is dysfunctional. ([2, p. 149]) The lateral cerebellar region is hypothesized to be responsible for the internal clock timing, and the medial region for the implementation of the timing of the body's motor system. Patients with lateral damage showed a higher standard deviation in clock timing as compared to patients with medial damage, and the opposite was true regarding motor delay.([5, p. 191]) Thus, another significant sign of cerebellar disease is altered timing of either the internal timekeeper system, or the motor implementation mechanism.

Chapter 3

Laptop based Assessment of Upper Limb and Finger Ataxia

3.1 Motivation

Cerebellar dysfunction is most often assessed qualitatively. For example, physicians often rate ataxia as “mild”, “moderate”, or “severe” failure to perform certain standard movements correctly. Qualitative assessments, however, are subjective and do not provide an ideal basis for the comparison of the efficacy of treatments or the correlations of assessments by two different doctors.

To provide a better basis for comparison, semi-quantitative tools such as the International Cooperative Ataxia Rating Scale (ICARS) and the Modified International Cooperative Ataxia Rating Scale (MICARS) have been developed ([9]) to provide a standardized metric for the assessment of cerebellar dysfunction. However, the scoring in these systems is still quantized to only four levels and is dependent on the experience of and the observations made by the tester.

The computerized assessment tool developed here provides an objective continuously valued assessment function. It makes the assessment devoid of subjective bias introduced by the tester and reduces the ability for variation in test administration. Continuously valued scoring makes it easier to note slight changes in a person’s condition. Computerized assessment also provides easy to manage as well as immediate

data storage, analysis, and scoring. Since the tests are developed in software, it allows for future upgrades to be made easily, as well as the ability to define and change the parameters of a test, or the components of a test suite.

A laptop was chosen as the target platform for administering the test, as it is a portable device that can be used both in clinics and in field studies, and generally has a standard user interface.

3.2 Design of Tests for the Laptop

A set of tests was developed to cover a range of cerebellar ataxia and timing dysfunctions such as impaired control of rhythmicity, speed and accuracy, and interdigit coordination of movement. The tests have been designed in a modular manner to allow for a tester to match up combinations of tests to create test suites. The number of tests administered in a test suite can be changed to allow for observation of learning effects, if any, and to determine a number of tests such that fatigue does not influence the results. There is also a practice test option, in which data is not recorded so that a subject may become comfortable with the test first. Also, parameters governing the test such as the intervals between cues, number of cues, etc. can be modified by the creator of the test suite to find the parameters that optimize the testing ability of a particular test suite. Default values were chosen by talking to Dr. Steve G. Massaquoi and Dr. Jeremy D. Schmahmann.

3.3 Tests Developed

3.3.1 Time Keeper vs. Implementation System

a) Internal Pacing

This test consists of providing a cue of 10 beep tones at regular intervals to a subject. The subject is then expected to continue striking the <Enter> or <Backspace> bar at the same rate as the cues. The test suite designer can designate the interval length between the cues, and the number of keystrokes the subject should supply

after the cues have ended. The default values are 0.5 seconds for the interval length, and 20 keystrokes to be recorded.

b) External Pacing

This test consists of a subject being asked to strike the <Enter> or <Backspace> key every single time he or she hears a beep. The test suite designer can designate the interval length between the cues, and the number of cues. The default values are 0.5 seconds for the time interval length and 20 for the number of cues.

These two tests were developed with the model developed by Wing and Kristofferson in mind. It is hypothesized that the lateral cerebellum is involved in internal clock timing, and the medial cerebellum in implementation of motor execution. Thus, a person with a lateral cerebellar lesion would be expected to have a high variance for the intervals for the internal pacing test, but have a low variance for the external pacing test. A person with a medial cerebellar lesion would be expected to have a high variance for both the internal and external pacing tests.

After designing these two tests, it was realized that even though the external pacing test provides cues at regular intervals, subjects might use an internal pacing strategy to accomplish the task. Therefore the test may not be used to accurately assess a subject's reaction time, which is thought to be prolonged in certain cerebellar system disorders. To address this issue, a third, random external pacing test was created. In this test, a subject is provided with cues at random interval lengths ranging from 0.5 to 1.0 seconds, and is instructed to hit the <Enter> or <Backspace> key whenever he or she hears a beep. This helps prevent a subject from using an internal pacing strategy for completing the test to provide a better measure of reaction time.

3.3.2 Rhythmicity, Interdigit Coordination, and Single Limb Speed/Accuracy tradeoff

c) One Finger GH Pressing

This test consists of a subject being asked to strike the adjacent "G" and "H" keys

alternately as fast as possible while trying to keep a regular rhythm using the index finger. The interval between each keypress is recorded, as well as the keys pressed. The test designer can designate the number of keypresses to be recorded.

d) Two finger GH Pressing

This test consists of a subject being asked to strike the “G” and “H” keys as fast as possible while trying to keep a regular rhythm using the index finger for the “G” key and the middle finger for the “H” key. The interval between each keypress is recorded, as well as the keys pressed. The test designer can designate the number of keypresses to be recorded.

These two tests allow for the assessment of a subject’s speed and variability over the intervals, as well as his or her ability to accurately alternate between the “G” and “H” keys. The reason for the two different tests is that it is possible that the coordination between two different digits is implemented differently than the control of a single digit. It is known that fine isolation of individual finger movements depends on the integrity of the cerebral cortex. Therefore, cortical selection mechanisms may be more important in the second test. Therefore, the two finger test may help differentiate between different subtypes of coordination dysfunction.

e) One Finger DL pressing

This test consists of a subject pressing the “D” and “L” keys as fast as possible with the index finger while keeping the arm from the shoulder to the finger completely straight and rigid if possible. A constant bend in the wrist is allowed as long as the arm is kept rigid. The interval between the key presses and the actual keys pressed is recorded. The test designer can designate the number of keypresses to be recorded.

These measurements allow for a speed and accuracy measurement, the trade-off for which is hypothesized to be extremely significant for cerebellar ataxia in comparison to other CNS disorders.

3.4 Software Design

The software was designed with the consideration that most of its users may not have extensive computer experience. A Graphical User Interface(GUI) based in MATLAB was used. Figure 3-1 shows the main program menu.

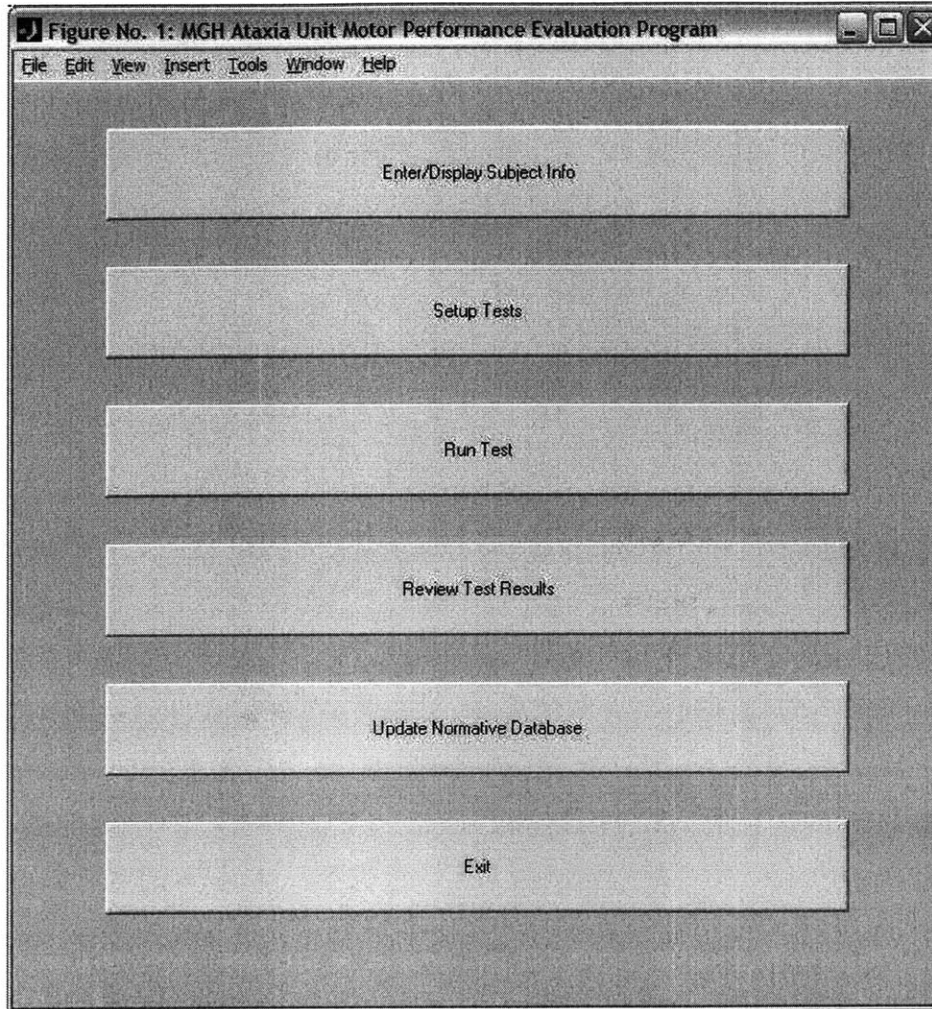


Figure 3-1: Laptop Main Program Menu
This is the main menu for the laptop testing program.

Under “Enter/Display Subject Info”, a user has the ability to enter new subject information, or display an already defined subject’s information. The program assigns the subject a number associated with a letter, under which the subject’s information will be recorded. This helps provide patient anonymity during data storage and

analysis, but still provides a method to trace the data back to its source.

Under the “Setup Tests” option, the tester has the ability to design test suites. They can be saved under a variety of names, allowing different tests to be designed for specific purposes or subjects. In setting up the test suite, the number of trials of each test, the order of the tests, and the parameters governing the test can be set. The window in which these parameters can be set is shown in Figure 3-2.

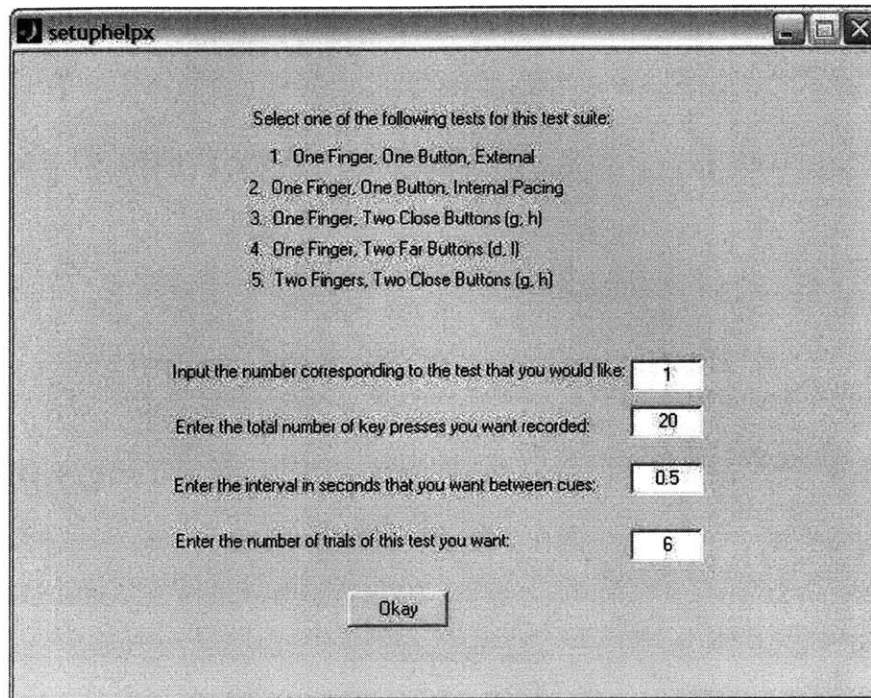


Figure 3-2: Test Setup Window

This window allows a tester to select the test to be administered in a given test suite, and the parameters governing the test. The values shown above are the default values determined through discussions with Dr. Massaquoi and Dr. Schmahmann.

The run test option allows a previously designed test suite to be run. The subject’s last name is asked for in order to verify that the data will be recorded under the appropriate subject number, and will thus be able to be accurately traced back if so needed. The examiner has the ability to allow a subject to take practice tests in which the data is not recorded, thus allowing for a person to take tests until the examiner feels that the subject understands what is being asked of him or her, and feels comfortable taking the test. Once the practice tests are over, the actual test is

run. The data is then recorded under the subject number, associated with the date and trial number. At the end of all the trials for one test, the data is compiled under a total data file.

The data collected can then be viewed almost immediately in the “View Test Results” option. Figure 3-3 shows the results of an external pacing test.

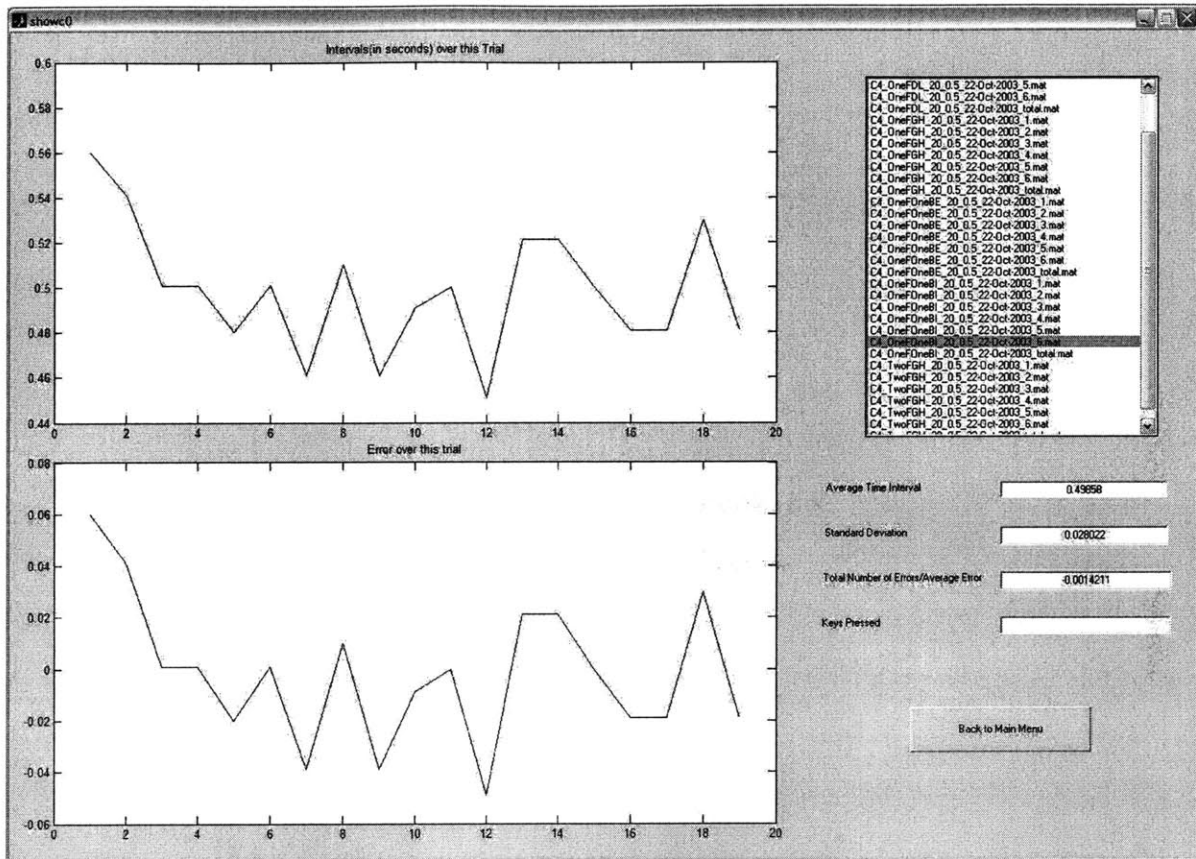


Figure 3-3: Data Display Window

This window allows results for a particular subject number to be viewed.

As can be seen in Figure 3-3, the results are shown by subject number, so that from this screen, no association can be made to the identity of the patient. The top right window gives a list of data files that some one may wish to view the results of. The average interval, standard deviation for the intervals, errors made, and the keys hit are displayed on the right with graphs of the intervals and error on the left.

The “Update Normative Database” option has not been linked to a function yet,

but will be linked to an analysis function that has been tested and proves to be an effective method for analysis. Since a scoring system is still being developed, when controls are tested, their results can be compiled into a database as to find the best dividing function between controls and patients.

3.5 Experimental Procedures

Most of the data was collected at Massachusetts General Hospital (MGH). Controls and patients of ages ranging from 21 through 58 and 9 through 75 respectively were tested. Each subject took a test suite consisting of 6 trials of each of the tests, with 20 key hits recorded for each one. Intervals for pacing times were specified as being 0.5 seconds. Practice tests were not allowed for these sessions, so that if there was a learning effect, it could be observed and recorded to derive a specification on how many trials should be considered adequate for practice. For the DL test, people were instructed to go as fast as they could, so that they would make some errors, so that there would be no floor effect. If the subject were pushed to a speed where he or she was making some errors, then a speed accuracy relationship could be more accurately derived for the given subject.

3.6 Results and Analysis

Data from 19 controls and 67 patients was analyzed.

The results of the the testing were plotted by subject number vs. the average time interval taken by the subject for a test, with bars indicating the variance around each point.

3.6.1 DL Testing

The results of the DL testing are shown in Figure 3-4, where the average time to move between the “D” and “L” key is plotted for each subject. Data from controls are depicted as “+” and from patients are depicted as “□”. Each data point has a

bar showing $\pm\sigma_{intervals}$. From this graph, one can see that the average movement time for patients generally tends to be higher, as well as the standard deviation for their intervals, indicating a higher variance in patients' rhythmicity.

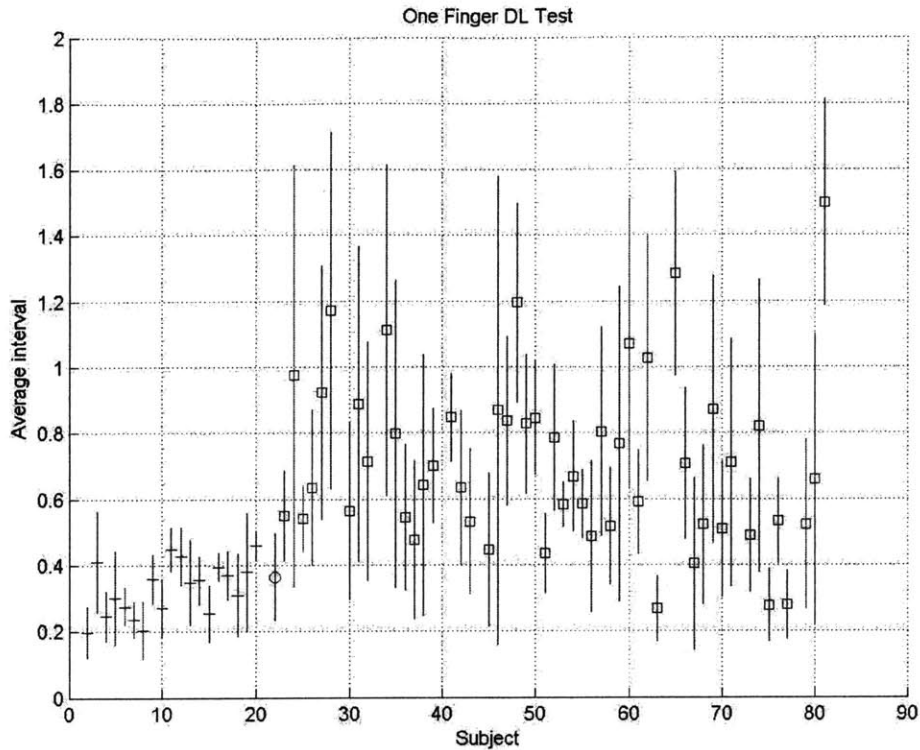


Figure 3-4: Average Time Interval for DL testing

This graph shows the average movement time to move between the “D” and “L” keys. Controls are depicted as “+” and patients are depicted as “□”. Each data point has a bar showing $\pm\sigma_{intervals}$. From this graph, it seems that the movement time for patients generally tends to be higher, as well as the standard deviation for their intervals, indicating a higher variance in patients' rhythmicity.

Further speed accuracy analysis was done on the DL key pressing results. It was not done on the GH pressing tests, because after talking to the test administrator, it was discovered that the key repeat option had not been disabled during testing, thus making it hard to judge if a repeated key press was an error or a subject holding a finger on a key too long.

Errors were computed for the DL test as follows. All the keypresses that were not “D” or “L” were removed from the array. Then the remaining array was searched for

the consecutive “DL.” The number of errors, num_errors , was considered to be the difference between the total number of key presses (usually set to twenty) and twice the number of consecutive “DL”’s found, num_DL , as shown in the equation 3.1.

$$num_errors = 20 - 2 * num_DL \quad (3.1)$$

In computing the average movement time, intervals that were less than 0.05 seconds were discounted from the averaging process, as it probably meant that it was due to the subject striking two adjacent keys nearly simultaneously. If such intervals were counted as the time to make two separate key strokes, the average interval for the test would appear lower than the actual value if the person made a lot of inaccurate hits, thus skewing the data. Data over the 6 trials was averaged to generate a single score for a subject.

Equation 3.2 from [1] is shown below.

$$MovementTime = a + b * \log\left(\frac{1}{error}\right) \quad (3.2)$$

Based on Equation 3.2, laptop performance scores, P_DL and C_DL were then created for each patient and control respectively by weighting the error and the average movement time according to Equations 3.3 and 3.4 respectively.

$$P_DL = \left| \left(2 + \log\left(\frac{1}{\mu_{num_errors}}\right) - 7 * \mu_{movementtime} \right) \right| \quad (3.3)$$

$$C_DL = \left| \left(2 + \log\left(\frac{1}{\mu_{num_errors}}\right) - 7 * \mu_{movementtime} \right) \right| \quad (3.4)$$

The log of $\frac{1}{\mu_{num_errors}}$ was used modeling it after the relationship found by Fitts and Peterson in [1]. The average movement time over 6 trials, $\mu_{movementtime}$, was weighted by a factor of 7, as it produced the best correlation with previous scoring systems. The variable μ_{num_errors} represents the average number of errors over 6 trials. A bias of 2 was added to the equation to shift the data points in the first quadrant of the Cartesian plane.

These P_DL scores were then compared to other scoring schemes. One such com-

parison was made to MICARS scoring¹, and the subcategories of its scoring. Correlations were found to be 0.7359 with total MICARS scores and 0.7351 with the subcategory of MICARS arm scores. Figures 3-5 and 3-6 show P_DL plotted against the total MICARS scores and the MICARS arm scores respectively.

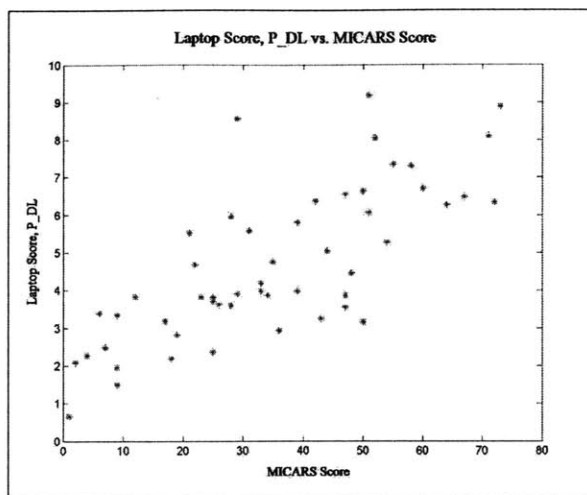


Figure 3-5: Laptop Score, P_DL vs. MICARS Score

The laptop scores for the patients, P_DL, have a correlation of 0.7539 with the MICARS scores.

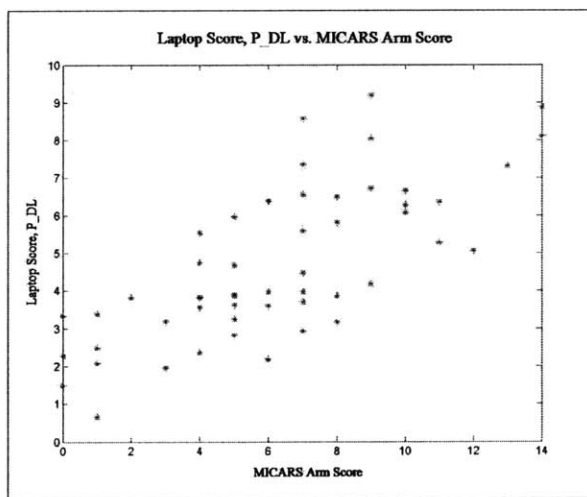


Figure 3-6: Laptop Score, P_DL vs. MICARS Arm Score

The laptop scores for the patients, P_DL, have a correlation of 0.7351 with the MICARS arm scores.

¹The MICARS scoring scheme is a set of questions in which a subject is rated using discretized integer scores.

The z-scores ², Z_DL were computed for each patient i, using the Equation 3.5.

$$Z_DL(i) = \frac{P_DL(i) - \mu_{C_DL}}{\sigma_{C_DL}} \quad (3.5)$$

In Equation 3.5, Z_DL is the z-score, P_DL is the laptop score, μ_{C_DL} is the average value for the laptop scores for the controls, and σ_{C_DL} is the standard deviation for the laptop scores for the controls.

Figure 3-7 shows $\frac{1}{\mu_{num_errors}}$ plotted versus the average movement time, with each data point representing an individual subject. Lines depicting the z-scores are included.

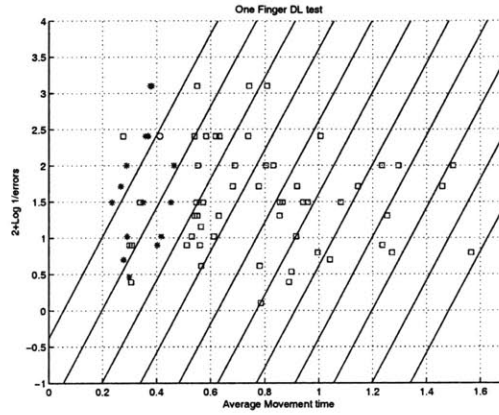


Figure 3-7: Z-Score Divisions

The lines shown correspond with z-scores of -1 to 9. Most patients have a z-score greater than 1.

Most patients have a z-score higher than 1.

3.6.2 Tests a-d

Preliminary analysis was done on the rest of the tests.

For the internal pacing test, as shown in Figure 3-8 each subject was plotted vs. his or her average error for each interval, i.e. how far off he or she was from the desired 0.5 second interval. Error bars depict the standard deviation of all the intervals for a particular subject.

²Z-scores are the deviation of a number from the mean, normalized by the standard deviation.

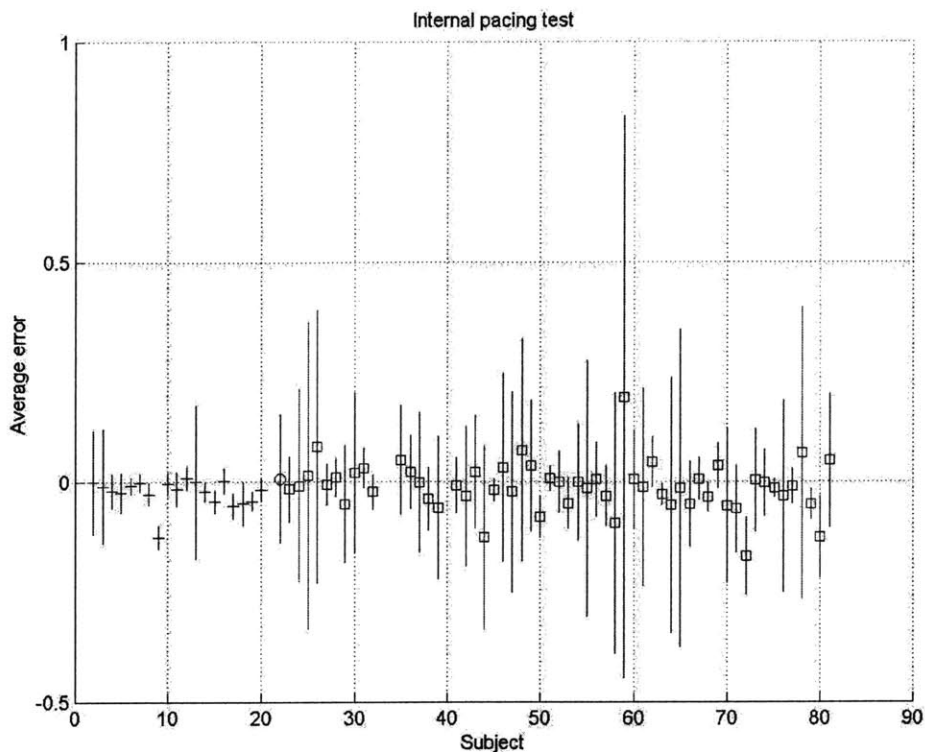


Figure 3-8: Internal Pacing Test

The average error for each interval is plotted for each subject. The error lines around each data point indicate the magnitude of the standard deviation of the error. Controls are depicted as “+” and patients are depicted as “□”. A trend that can be noted from this image is that most patients have a higher standard deviation than the controls, indicating that they have a higher variance between each interval, which is consistent with results seen and predicted by [2] and [5].

In looking at Figure 3-8, a trend can be noted that most patients have a higher standard deviation than the controls, indicating that they have a higher variance between each of the intervals, which is consistent with results seen and predicted by [2] and [5].

Similarly, for the external pacing test, as shown in Figure 3-9 each subject was plotted vs. his or her average error for each interval, i.e. how far off he or she was from the desired 0.5 second interval. Error bars depict the standard deviation of all the intervals for a particular subject.

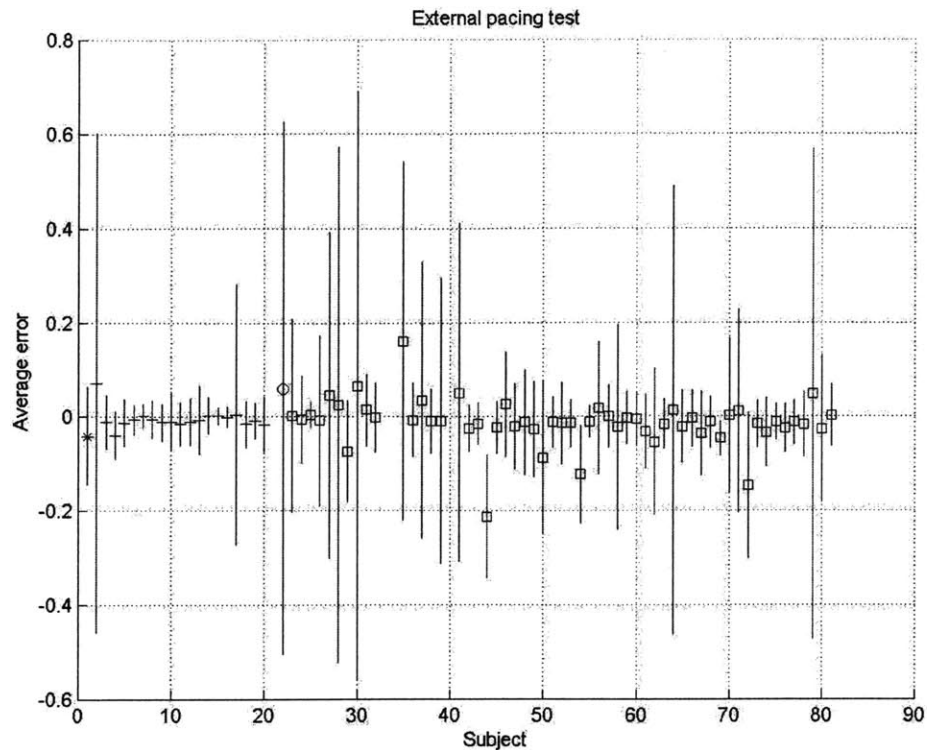


Figure 3-9: External Pacing Test

The average error for each interval is plotted for each subject. The error lines around each data point indicate the magnitude of the standard deviation of the error. Controls are depicted as “+” and patients are depicted as “□”. The same trend as in the internal pacing test is present in which most patients have a higher standard deviation than the controls, indicating that they have a higher variance between each interval, which is consistent with results seen and predicted by [2] and [5].

The same trend as found in Figure 3-8 can be seen in Figure 3-9, in which most patients have a higher standard deviation than the controls, indicating that they have a higher variance between the each of the intervals, which is also consistent with results seen and predicted by [2] and [5].

Figure 3-10 shows the average time interval plotted for each subject for the “One Finger GH Test”. The errorbars show the standard deviation of the length of the time intervals for each movement.

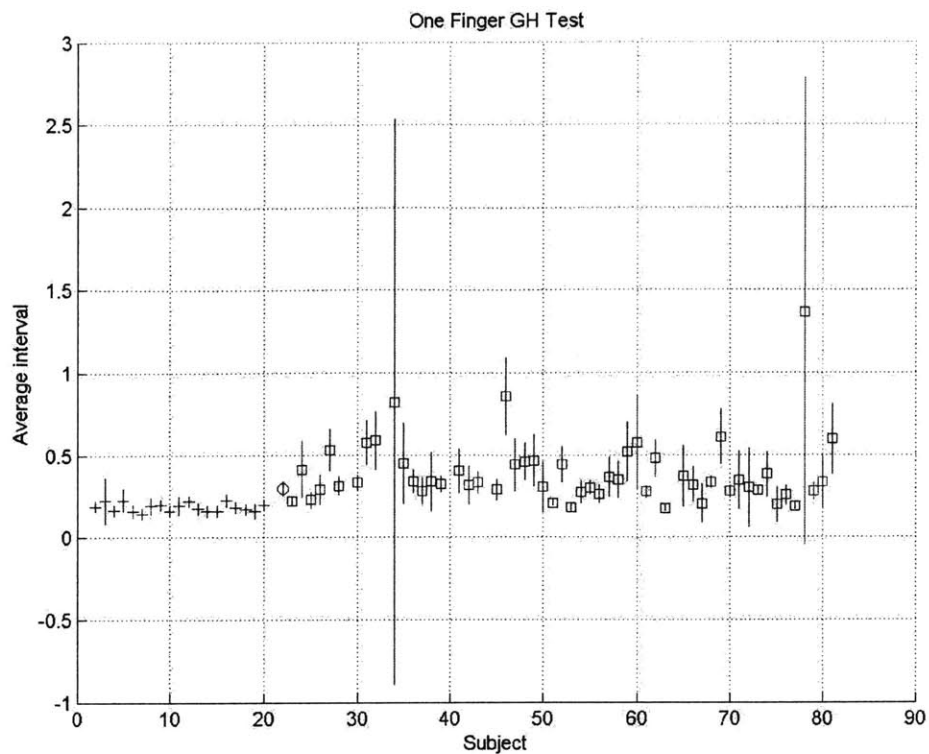


Figure 3-10: One Finger GH Test

The average time interval for each movement is plotted for each subject. The error lines around each data point indicate the magnitude of the standard deviation of the length of the intervals. Controls are depicted as “+” and patients are depicted as “□”. From the figure, one can see that patients generally have a higher movement time, and a larger variance in the length of their time intervals in comparison to the controls.

From the Figure 3-10, one can see that patients generally have a higher movement time, and a larger variance in the length of the time intervals for each movement.

Figure 3-11 shows the average time interval plotted for each subject for the “Two Finger GH Test”. The errorbars show the standard deviation of length of the time intervals for each movement.

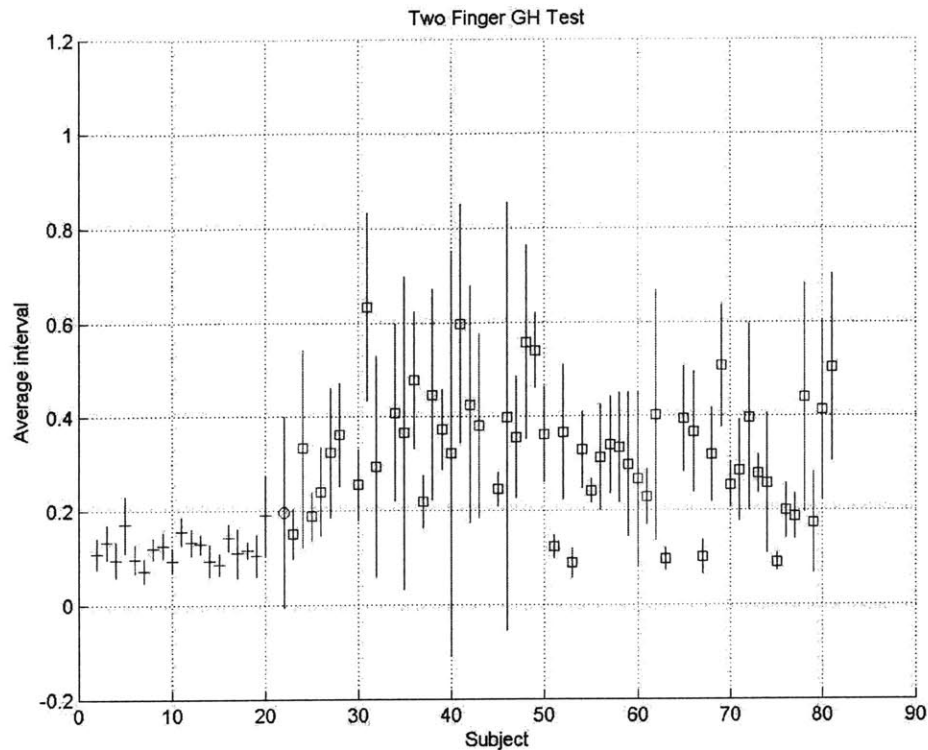


Figure 3-11: Two Finger GH Test

The average time interval for each movement is plotted for each subject. The error lines around each data point indicate the magnitude of the standard deviation of the length of the intervals.

Controls are depicted as “+” and patients are depicted as “□”. The trend is more vivid in comparison to the “One Finger GH Test” in which one can see that patients generally have a higher movement time, and a larger variance in the length of their time intervals in comparison to the controls.

In Figure 3-11, the trend is more vivid in comparison to the “One Finger GH Test” in which one can see that patients generally have a higher movement time, and a larger variance in the length of their time intervals in comparison to the controls.

Data for the random interval testing has not yet been collected.

Chapter 4

Manipulandum and Model Based Assessment of Upper Limb Ataxia

4.1 Motivation and Strategy

Though the laptop scoring system gives a quantitative assessment of motor performance error associated with cerebellar dysfunction, it does not give any understanding of why motor performance error occurs, or how it might be corrected. An engineering control-model based quantitative assessment may provide insight into the mechanisms underlying the observed behaviour. If there can be a fundamental understanding of cerebellar function, then there is a possibility for alleviating the symptoms as well as fixing the root cause of the problem.

A control model of the cerebellum in conjunction with a two joint arm (plant) model was used to simulate a point to point reaching movement. The results of the simulations were compared to real trajectories recorded using a low impedance manipulandum from a subject with cerebellar ataxia, as well as control subjects. The trajectories of ataxic and control subjects were fit using a model of the system by adjusting only the parameters associated with the cerebellar component of the model. If the model can be used to match the trajectories of both the ataxic and control subjects closely, then the model not only gives a quantitative description of the movement with cerebellar function and dysfunction, but may also give insight as

to how the function of the cerebellum has been affected by disease or degeneration.

4.2 Experimental Setup

A person was seated in front of the manipulandum as shown in Figure 4-1. Two targets were present on the table; one was the starting target, one was the ending target. Once the person had brought the manipulandum arm to rest at the starting target, the subject was instructed to move the manipulandum arm from the starting target to the ending target in as straight of a line as possible. The subject was coached to have two different movement speeds, one with a total movement time of about 1.2 seconds, and the other of about 0.7 seconds. The movement time of 1.2 seconds is the one that is primarily analyzed, as not all subjects could accomplish the movement in 0.7 seconds.

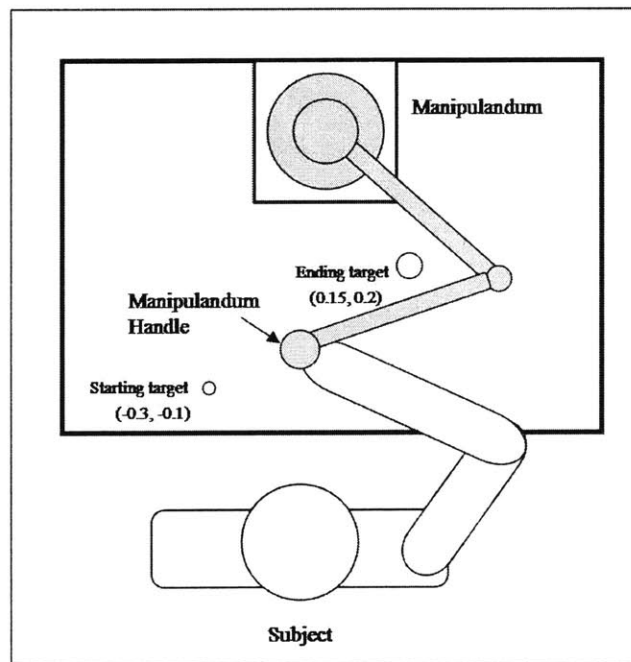


Figure 4-1: Manipulandum Test Setup

This shows the basic setup for collecting data using the manipulandum. The subject was asked to move the manipulandum handle from the starting point (with xy-coordinates $(-0.3, -0.1)$) to the target (with xy-coordinates $(0.15, 0.2)$).

Data collection was designed to begin when the subject had the manipulandum on target, had a positive velocity in the x and y direction, and exceeded a tangential speed of 0.005 meters/second. Data collection stopped when the manipulandum was over the target and had a tangential speed of less than 0.001 m/s. These limits helped reduce the recording of spurious motion at the beginning and the end of the test. Kinematic data was collected at a rate of 200 Hz, consisting of the Cartesian coordinates and Cartesian velocities of the manipulandum handle.

4.3 Model

The model shown in Figure 4-2 was used to simulate the point to point trajectories. This model was based on the Recurrent Integrator Proportional Integrator Derivative (RIPID) model described by [7] to explain the cerebellar stabilization of long-loop control of arm posture and movement in the presence of physiological delays. The version of this model that is used for the current analysis, that is shown in Figure 4-2, for simplicity and for the purposes of initial analysis, does not include the delays or the delay stabilization present in the RIPID model described by [7]. However, it does retain the PID control model of the cerebellum. The features of this model are described more in the following sections.

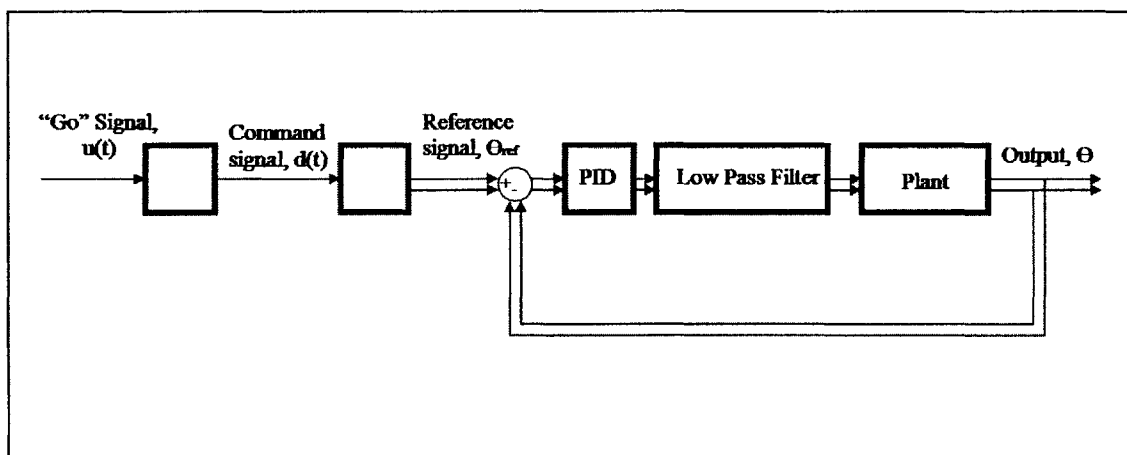


Figure 4-2: Overview of RIPID Model

This model was simulated to generate trajectories comparable to the ones obtained from subjects.

4.3.1 Model of Cerebral Interaction with Cerebellum

The cerebrum was modeled as providing a “go” signal, modeled as a unit step, $u(t)$. This step then generated a command signal, $d(t)$, which could be the step with the amplitude scaled in accordance to the total distance of the movement desired. To model more physiologic parameters, with less high frequency elements, the command signal was modeled as a sigmoidal distance vs. time function having the desired maximum velocity as its largest slope. Thus, the command signal was defined as the integral of Equation 4.1.

$$\dot{d}(t) = \frac{4 * v_{max}}{d_0^2} * (d_0 * u(t) - d(t)) * (d(t) + a_0 * u(t)) \quad (4.1)$$

In Equation 4.1, $\dot{d}(t)$ is the derivative of the command signal, $d(t)$. The maximum velocity of the movement is v_{max} , d_0 is the length between the starting and end point of the movement, $u(t)$ is the unit step “go” signal, and a_0 is a small constant allowing for movement from zero initial conditions, for which the value of 0.001 was used.

The command signal (the integral of Equation 4.1) was used to generate reference trajectories in the joint space as shown by Equations 4.2 through 4.8.

$$\theta_1(t) = \pi - \alpha_0(t) - \alpha_2(t) \quad (4.2)$$

$$\theta_2(t) = \pi - \cos^{-1} \left(\frac{currentpos(t)^2 - l_1^2 - l_2^2}{-2 * l_2 * l_1} \right) \quad (4.3)$$

$$\alpha_0(t) = \cos^{-1} \left(\frac{|x_{initial} + d(t) * \cos(\phi) - x_{sh}|}{currentpos(t)} \right) \text{ for } (x_{initial} + d(t) * \cos(\phi) - x_{sh}) < 0 \quad (4.4)$$

$$\alpha_0(t) = \pi - \cos^{-1} \left(\frac{|x_{initial} + d(t) * \cos(\phi) - x_{sh}|}{currentpos(t)} \right) \text{ for } (x_{initial} + d(t) * \cos(\phi) - x_{sh}) > 0 \quad (4.5)$$

$$\alpha_2(t) = \cos^{-1} \left(\frac{l_2^2 - currentpos(t)^2 - l_1^2}{-2 * currentpos(t) * l_1} \right) \quad (4.6)$$

$$currentpos(t) = \sqrt{(x_{initial} + d(t) * \cos(\phi) - x_{sh})^2 + (y_{initial} + d(t) * \sin(\phi) - y_{sh})^2} \quad (4.7)$$

$$\phi = \tan^{-1} \left(\frac{y_{final} - y_{initial}}{x_{final} - x_{initial}} \right) \quad (4.8)$$

4.3.2 Cerebellum

The error between the reference trajectory and the physical joint information fed back by the spinal cord is passed through the circuitry of the cerebellum which is modelled as a proportional integrator derivative(PID) controller. The derivative was modeled by Expression 4.9.

$$\frac{100s}{s + 100} \quad (4.9)$$

Expression 4.9 approximates the Laplace variable, “s” while providing a high frequency pole, thus attenuating very high frequency noise that a pure derivative function might elicit. The cerebellar PID control components were represented by three 2 by 2 gains matrices, Gb, Gk, and I1, which represented the gains for the derivative, proportional, and integrator controllers respectively.

4.3.3 Two Link Arm Model

Muscle Low Pass Filter

The output of the cerebellum then passes through a low pass filter that models the low pass property of muscle activation. Its cutoff is modeled around 30 radians per second similar to [7], as shown by Expression 4.10.

$$\frac{30^2}{(s + 30)^2} \quad (4.10)$$

Arm Model Parameters

The arm model that was used in the model to simulate any particular subject’s data was fitted to that particular subject. To accomplish this, physical measurements were taken just prior to collecting data. The measurements that were taken are depicted in Figure 4-3.

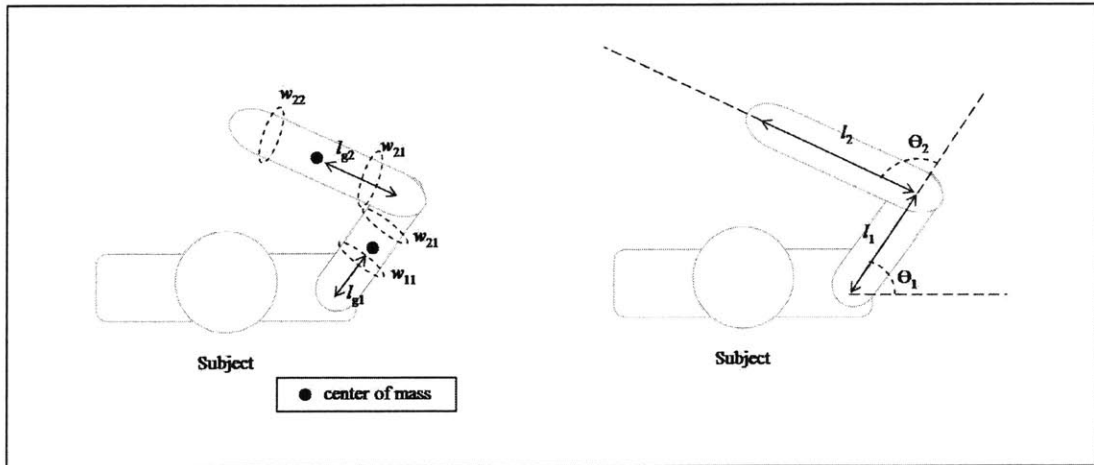


Figure 4-3: Diagram depicting Arm Model Parameters
 The parameters of the two link arm model are depicted in the above diagrams.

The length of the arm segment from the shoulder to the elbow, arm segment one, was measured as l_1 , and the segment from the elbow to the middle of the palm, arm segment two, was measured as l_2 . The circumference of arm segment one close to the shoulder was measured as being w_{11} and close to the elbow was measured as w_{12} . The circumference of arm segment two close to the elbow was measured as being w_{21} and close to the wrist was measured as w_{22} .

The arm segments were modeled as cylinders, of the average circumference for each arm segment, and of lengths l_1 and l_2 respectively. The formula for calculating the mass of arm segment one, m_1 , is shown in Equation 4.11.

$$m_1 = \left(\frac{w_{11} + w_{12}}{2} \right)^2 * \frac{1}{4 * \pi} * l_1 * 1000 \frac{kg}{m^3} \quad (4.11)$$

The equation for determining the mass of arm segment two, m_2 was symmetrical to Equation 4.11. The distance to the center of mass each arm segment, l_{g1or2} was obtained using Equation 4.12.

$$l_{g1or2} = \frac{l_{1or2}}{2} \quad (4.12)$$

Equation 4.13 is the equation that was used to calculate the moment of inertia for

arm segment one, h_1 . Equation 4.14 is the equation was used to calculate the moment of inertia for arm segment two, h_2 . Moment arms were considered to be constant.

$$h_1 = \frac{1}{4} * m_1 * \left(\frac{w_{11} + w_{12}}{2 * pi} \right)^2 + \frac{1}{l_2} * m_1 * l_1^2 \quad (4.13)$$

$$h_2 = \frac{1}{4} * m_2 * \left(\frac{w_{21} + w_{22}}{2 * pi} \right)^2 + \frac{1}{l_2} * m_2 * l_2^2 \quad (4.14)$$

The stiffnesses of the muscles were kept constant between subjects. The value for the stiffness for the shoulder, k_{sh} was 4, for the elbow, k_{el} was 1, and for the shoulder and elbow combination, k_{shel} was 2. Since the coordinate space for the arm model was in joint angle coordinates, these values were combined into a rotary stiffness matrix, R , as shown in Equation 4.15.

$$R = \begin{bmatrix} k_{sh} + k_{shel} & k_{shel} \\ k_{shel} & k_{el} + k_{shel} \end{bmatrix} \quad (4.15)$$

A similar approach was taken in modeling muscle viscosity. The value for the viscosity due to the shoulder, b_{sh} was 0.32, due to the elbow, b_{el} was 0.08, and due to the combination of the shoulder and the elbow, b_{shel} was 0.16. Combining it into a rotary viscosity matrix gave D according to Equation 4.16.

$$D = \begin{bmatrix} b_{sh} + b_{shel} & b_{shel} \\ b_{shel} & b_{el} + b_{shel} \end{bmatrix} \quad (4.16)$$

An inherent viscosity due to the soft tissues was also assumed, which gave rise to another viscosity matrix D_0 as described in Equation 4.17. The values used for these matrices are comparable to those used in [4].

$$D_0 = \begin{bmatrix} 0.032 & 0 \\ 0 & 0.008 \end{bmatrix} \quad (4.17)$$

Muscle activation can cause the stiffnesses and viscosities to change. Also, different people will usually have different stiffnesses and viscosities for the muscles in their arms. This is not accounted for in this model, as there is no simple way to account

for these changes. It is hoped that if the data can be fit well with this level of approximation, it will give enough insight that the exact value of the stiffnesses and viscosities for each person will not be required.

Limb Dynamics

The torque on arm segment one, τ_1 and on arm segment two, τ_2 are defined according to Equations 4.18 and 4.19 respectively.

$$\tau_1 = (h_1 + h_2 + 2m_2l_1l_{g2}\cos(\theta_2) + m_2l_1^2) * \ddot{\theta}_1 + (h_2 + m_2l_1l_{g2}\cos(\theta_2)) * \ddot{\theta}_2 - m_2l_1l_{g2}\sin(\theta_2) * \dot{\theta}_2^2 - 2m_2l_1l_{g2}\sin(\theta_2) * \dot{\theta}_1 * \dot{\theta}_2 \quad (4.18)$$

$$\tau_2 = (h_2 + m_2l_1l_{g2}\cos(\theta_2)) * \ddot{\theta}_1 + h_2 * \ddot{\theta}_2 + m_2l_1l_{g2}\sin(\theta_2) * \dot{\theta}_1^2 \quad (4.19)$$

These equations can be condensed to Equations 4.20 and 4.21.

$$\begin{bmatrix} \tau_1 \\ \tau_2 \end{bmatrix} = H * \begin{bmatrix} \ddot{\theta}_1 \\ \ddot{\theta}_2 \end{bmatrix} + C * \begin{bmatrix} \dot{\theta}_1 \\ \dot{\theta}_2 \end{bmatrix} + D_0 * \begin{bmatrix} \dot{\theta}_1 \\ \dot{\theta}_2 \end{bmatrix} \quad (4.20)$$

$$\begin{bmatrix} \tau_1 \\ \tau_2 \end{bmatrix} = R * \left(\begin{bmatrix} input_1 \\ input_2 \end{bmatrix} - \begin{bmatrix} \theta_1 \\ \theta_2 \end{bmatrix} \right) - D * \begin{bmatrix} \dot{\theta}_1 \\ \dot{\theta}_2 \end{bmatrix} \quad (4.21)$$

H is a 4 by 4 matrix which is a function of θ , defined in Equation 4.22, C is a 4 by 4 matrix that is a function of θ and $\dot{\theta}$, defined by Equation 4.23, R and D are the 4 by 4 stiffness and viscosity matrices respectively in rotary coordinates, previously defined in Equations 4.15 and 4.16, and the *input* is the output of the muscle low pass filter.

$$H = \begin{bmatrix} h_1 + h_2 + 2m_2l_1l_{g2}\cos(\theta_2) + m_2l_1^2 & h_2 + m_2l_1l_{g2}\cos(\theta_2) \\ h_2 + m_2l_1l_{g2}\cos(\theta_2) & h_2 \end{bmatrix} \quad (4.22)$$

$$C = \begin{bmatrix} -2m_2l_1l_{g2}\sin(\theta_2)\dot{\theta}_2 & -m_2l_1l_{g2}\sin(\theta_2)\dot{\theta}_2 \\ m_2l_1l_{g2}\sin(\theta_2)\dot{\theta}_1 & 0 \end{bmatrix} \quad (4.23)$$

The equations were manipulated to solve for θ and $\dot{\theta}$, which are the vectors containing the output joint angles and joint velocities.

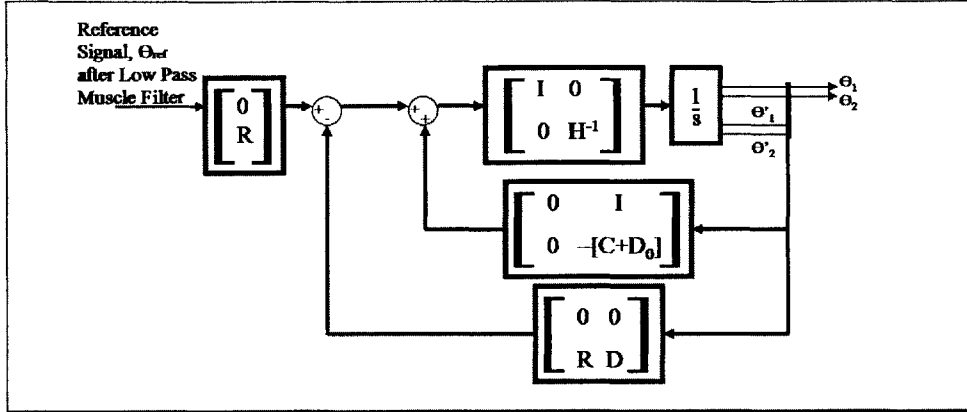


Figure 4-4: Implementation of Two Link Arm Model

The diagram shows how the two link arm model was implemented to produce joint angles for the model system.

The two link arm model was then implemented as shown in the block diagram in Figure 4-4. The output θ was then fed back to be compared to the reference trajectory, with the error signal being amplified/attenuated by the gains to help the plant follow the reference trajectory.

4.3.4 Conversion from Joint to Cartesian Coordinates

Since the data was collected in Cartesian coordinates, the model's output joint angle coordinates were converted to Cartesian coordinates using Equations 4.24 and 4.25, so that the model's output could easily be compared to the data to assist in adjusting the cerebellar gains to find good fits.

$$x = l_1\cos(\theta_1) + l_2\cos(\theta_2 + \theta_1) + x_{sh} \quad (4.24)$$

$$y = l_1 \sin(\theta_1) + l_2 \sin(\theta_2 + \theta_1) + y_{sh} \quad (4.25)$$

To find the x and y velocities from the model, the following Equations 4.26 and 4.27 were used.

$$\dot{x} = -l_1 \sin(\theta_1) * \dot{\theta}_1 - l_2 \sin(\theta_2 + \theta_1) * (\dot{\theta}_2 + \dot{\theta}_1) \quad (4.26)$$

$$\dot{y} = l_1 \cos(\theta_1) * \dot{\theta}_1 + l_2 \cos(\theta_2 + \theta_1) * (\dot{\theta}_2 + \dot{\theta}_1) \quad (4.27)$$

4.3.5 Evaluating Fits of Trajectories

To evaluate the quality of the model's output to the data collected, the *Rsquared* was calculated according to the function defined in Equation 4.28.

$$Rsquared = 1 - \frac{error_{speed}^2 + 100 * error_x^2 + 100 * error_y^2}{total_{speed}^2 + total_x^2 + total_y^2} \quad (4.28)$$

The speed, x values, and y values of the model and data were arrays that were functions of time in Equation 4.28. The path trajectory error was weighted more heavily than the speed error, but both speed and path errors were used to evaluate the quality of the fits.

4.4 Experimental Subjects

Horizontal planar trajectories were studied in 4 male subjects ranging from 23-50 years of age, as shown in Table 4.1. Subjects 1 and 4 had been diagnosed by Dr. Massaquoi as having mild to moderate ataxia, and both had Magnetic Resonance Images (MRIs) that showed degeneration of the cerebellum only.

Subject	Ataxic?	Age	Weight
P1	Yes, can walk.	27	85kg
P2	Yes, cannot walk	50	88.5kg
C1	No	23	79.4kg
C2	No	31	79.4kg

Table 4.1: Subject Overview

The parameters for the subjects that were measured to fit the arm model to each subject are shown in Table 4.2.

Subject	l_1	l_2	w_{11}	w_{12}	w_{21}	w_{22}	x_{sh}	y_{sh}
P1	0.3556m	0.36195m	0.3302m	0.3048m	0.2794m	0.19685m	0.06m	-0.38m
P2	0.3556m	0.3429m	0.4m	0.3m	0.3m	0.2m	0.08m	-0.45m
C1	0.3429m	0.381m	0.3937m	0.2921m	0.2921m	0.20955m	0.06m	-0.4m
C2	0.33655m	0.3556m	0.4318m	0.3048m	0.2921m	0.2032m	0.06m	-0.23m

Table 4.2: Subject Parameters

The masses and moments of inertias calculated for all the subjects are shown in Table 4.3. The masses of the arms seem to be slight overestimates as they are considered to be the density of water throughout, while their density is probably less. These values differ by about a factor of 2 in comparison to the values used in [4], which was consistent and seems reasonable for the purposes of this analysis.

Subject	m_1 (kg)	m_2 (kg)	h_1 ($\cdot kgm^2$)	h_2 ($\cdot kgm^2$)
P1	2.8526	1.6332	0.0316	0.0182
P2	3.4665	1.7054	0.0392	0.0174
C1	3.2084	1.9075	0.0338	0.0238
C2	3.6328	1.7355	0.0362	0.0187

Table 4.3: Subject Arm Masses and Moments of Inertia

4.5 Results

Typical recorded trajectories looked like the trajectories shown in Figures 4-5 and 4-6.

From initial cursory comparison of these two trajectories, it can be noted that the trajectory shown in Figure 4-6 is more curved than the trajectory in Figure 4-5. This seemed to be typical of patient trajectories in comparison to control trajectories, in which patient trajectories tended to overshoot the ending point and be less linear.

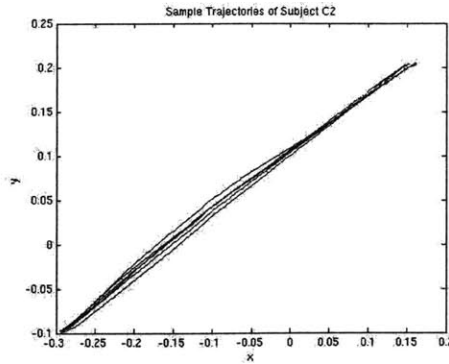


Figure 4-5: Sample Path Trajectories from a Control Subject
 These are 6 typical path trajectories recorded from a control subject.

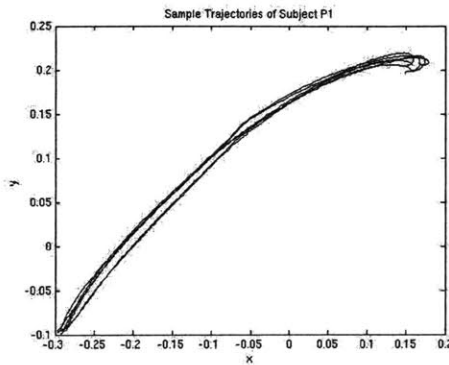


Figure 4-6: Sample Path Trajectories from a Patient Subject
 These are 6 typical path trajectories recorded from a patient subject.

4.5.1 Fitting the Trajectories

The gains of the cerebellum part of the model were modified to fit the trajectories. The maximum observed velocity from the data was used as the reference v_{max} for the model. The gains were modified by hand, or sometimes, a MATLAB script plotting the results of different gain combinations was utilized to help find a good fit. Three trajectories that seemed representative of the data set of similar speed were fit for each subject. Scripts using a MATLAB non-linear optimizer would result in a low value for absolute error, however, the resulting trajectory from the model would oscillate around the recorded data trajectory. The *Rsquared* values for the fits are shown in

Table 4.4.

Subject	$R_{squared_1}$	$R_{squared_2}$	$R_{squared_3}$
P1	0.9122	0.8949	0.8626
P2	0.8922	0.8566	0.8885
C1	0.9038	0.8451	0.7981
C2	0.9862	0.9819	0.9784

Table 4.4: $R_{squared}$ values for Trajectory Fits

Sample fits of path trajectories as well as the respective speed profiles are shown in Figures 4-7 through 4-8.

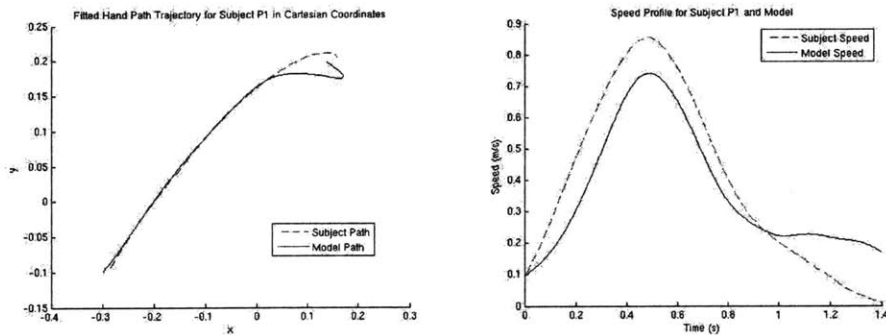


Figure 4-7: Fitted Path Trajectory and Speed Profile of Subject P1 with Model
 Subject P1 was mildly ataxic. Notice the small hook around the ending point indicative of a small overshoot. Though this simple model was unable to match the hook at the end, it is possible that a more detailed version of the model would be able to account for it.

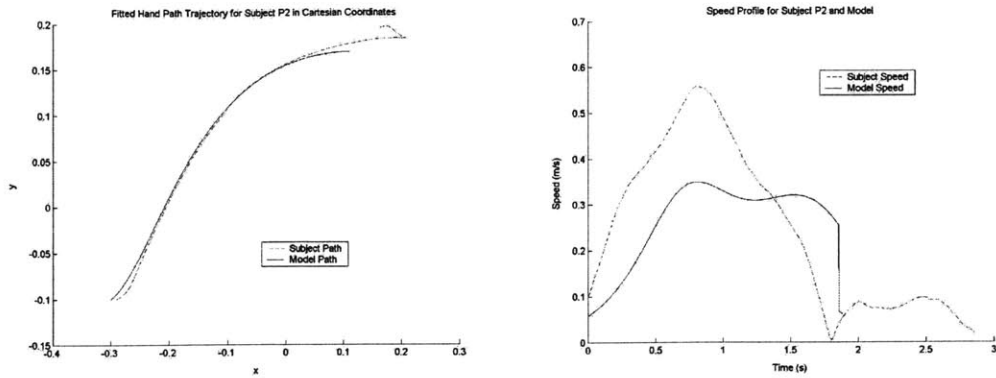


Figure 4-8: Fitted Path Trajectory and Speed Profile of Subject P2 and Model
 Subject P2 seemed to be moderately ataxic. This trajectory is much less linear compared to all the other subjects, and has an almost sigmoidal shape to it, with a very visible overshoot and hook back to the ending point. This was typical of all the trajectories for this subject. This subject found it difficult to move very fast, or to accomplish the task at higher speeds. The velocity fit is not as good as the other subjects' fits, however, it improved when the reference maximum velocity was increased above the observed maximum velocity.

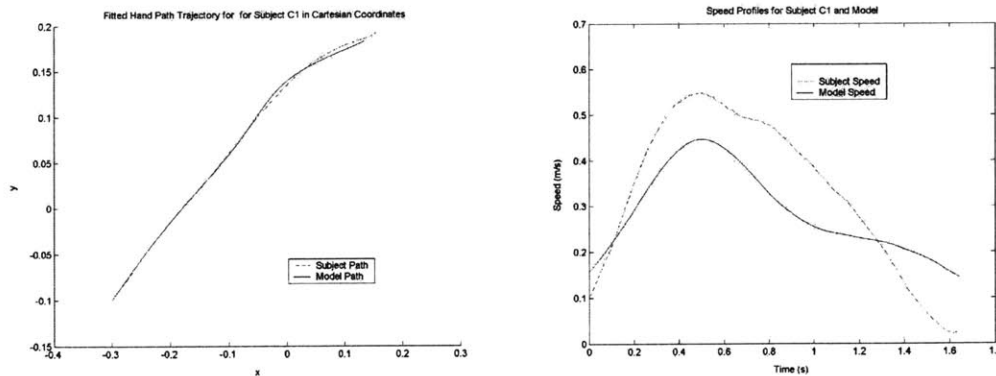


Figure 4-9: Fitted Path Trajectory and Speed Profile of Subject C1 with Model
 Subject C1 was a control subject. Though the actual trajectory wavers a bit, there is no overshooting hook near the ending point of the trajectory.

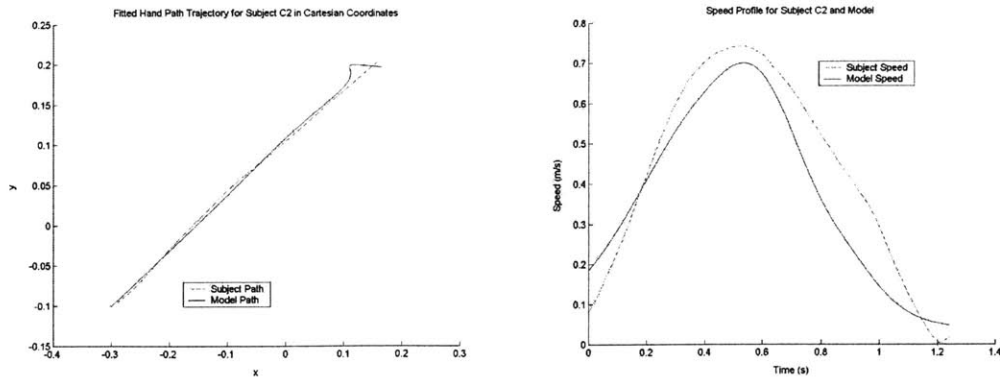


Figure 4-10: Fitted Path Trajectory and Speed Profile of Subject C2 with Model
 Subject C2's trajectory is more linear than that of Subject C1, however, similar to Subject C1's trajectory, it reaches the ending point without any noticeable overshoot.

In fitting the trajectories, the maximum observed velocity from the data was used as the reference v_{max} for the model. All the velocities generated by the model have a lower peak than the desired maximum. It is suspected that there is a larger difference between the reference and observed maximum velocities in ataxic patients. There reference signal was not directly measured in this experiment, so it is hard to make a direct comparison in this regard between controls and patients. It should be noted, however, that as the v_{max} used to try and fit Subject P2's trajectory was increased from the observed maximum velocity, the fits seemed to improve more than in comparison to fits of other subjects' trajectories. This suggests and supports that the degeneration of the cerebellum can cause a person to conduct a movement much slower than desired, thus creating a larger difference in the observed and reference maximum velocities of a movement.

The values for the gains matrices, G_b , G_k , I_1 , found for the fits for 4 subjects are shown in Figures 4-11 through 4-13.

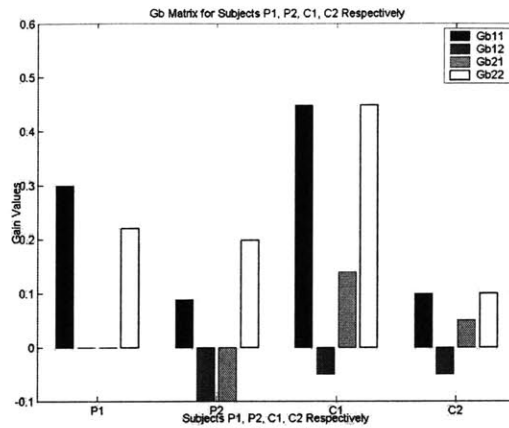


Figure 4-11: Gb

There seems to be a trend that the on-diagonal terms for the patient gains for Gb are asymmetric in comparison to the controls.

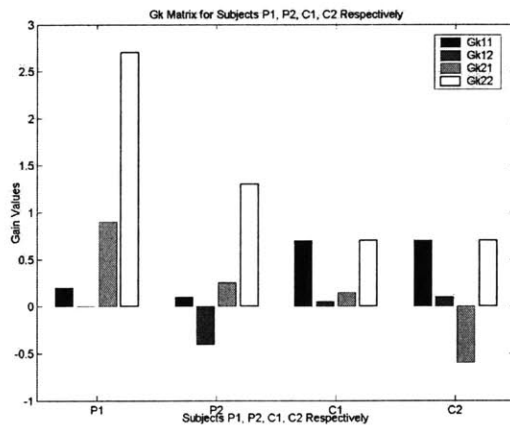


Figure 4-12: Gk

The asymmetry of patient gains in comparison to controls as seen with Gb can also be seen here with Gk as well. There also seems to be a trend in which Gk_{11} and Gk_{12} seem to be lower, and Gk_{21} and Gk_{22} seem to be higher for patients in comparison to controls.

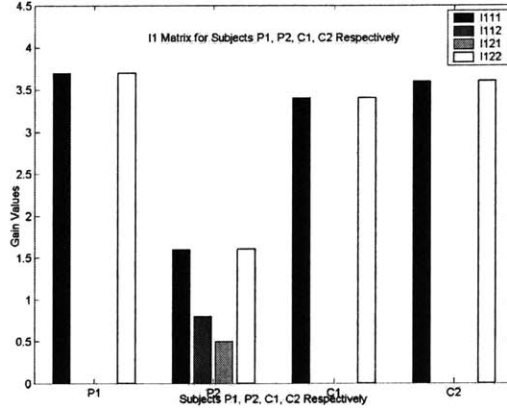


Figure 4-13: I1

I1 seems to be symmetric for all subjects. More prominent ataxia seems to decrease the gains for the on-diagonals; however this trend as well as aforementioned trends would need to be strengthened with a larger set of subjects.

In general, the earlier part of the trajectory was much easier to fit than the end of it. There were slight complications in the fits, as it is not known what the reference velocity for a patient is, as it is hypothesized that the observed velocity would be different than the hypothesized velocity due to incorrect following. The gains also changed from subject to subject depending on their physical parameters such as mass and arm lengths. This tended to change the absolute value of the gains, but the pattern of asymmetry for Gb and Gk for the patients seemed to remain consistent. Also, since the fits were of different qualities as can be seen by the *Rsquared* values, it is difficult to ascertain if the gains found for the exact same quality of fits would compare in the same manner as depicted in Figures 4-11 through 4-13.

Originally, there had been stipulation that ataxia would effect the magnitude of the gains by reducing them, however, no clear trend is visible from the data. From observing Subject P2, it was noted that there seemed to be speed limiting factor, that even though the Subject was trying to move faster, still could not move at the faster speed. If ataxia limits the speed that a person can move with, even though their intended speed is much higher, that would lead to the fact that the model should have been simulated with much higher v_{max} 's than observed. This may cause the

gains needed to fit those trajectories with higher v_{max} 's to be lower than calculated with the observed maximum speeds. Reduction in gain would cause movements to be less accurate, the asymmetry noticed in the gains suggests that ataxia may hinder joint coordination as well.

To try and compensate for the different sizes of the subjects, the stiffnesses and viscosities of the patients were normalized in proportion to the masses of the arms for each subject. However, when analyzed, the fits of the trajectories and the associated gains did not change significantly. Also, since it is a non-linear system, it is possible that there is another set of gains that corresponds to the same quality of fits. It may be worthwhile to analyze the quality of the fits for all possible combinations of the gains.

Chapter 5

Conclusions

Two quantitative assessment tools for the measurement of cerebellar dysfunction have been explored, that may prove to be useful tools in comparing cases and treatments of cerebellar dysfunction.

The scoring results of the laptop test correlate well, (0.7359), with existing scoring systems such as MICARS. It provides a tool that might help in clinical assessment of patients. Further developments can be made to see how many tests are needed for an accurate assessment by comparison of the variability within the test sets. Also, the learning effect on the accuracy and speed on the execution of a simple rhythmic movement, if there is any, and the average amount of trials it takes for the results to start being consistent could be quantified and calculated. Also, by testing the same people over again, the consistency of scores could be determined. Another test is to figure out what parameters are optimal for testing the severity of conditions and picking out signs for subtypes of cerebellar disease.

In fitting subject trajectories with a model, trends of asymmetry were noted in the G_b and G_k matrices of patients in comparison to controls. There were also trends noted of Gk_{11} and Gk_{12} being lower, and Gk_{21} and Gk_{22} being higher for patients in comparison to controls. A larger set of subjects and subject data will help evaluate the validity of these trends. Also, finding a wider range of gains as possible solutions to match a trajectory, and incorporating other elements into the model, such as delays, and non-constant stiffnesses and viscosities may help make trends more apparent.

Firmly establishing trends associated with cerebellar dysfunction may hopefully help in the development of new treatments for cerebellar disorders.

Bibliography

- [1] P[aul] M. Fitts and J[ames] R. Peterson. Information capacity of discrete motor responses. *Journal of Experimental Psychology*, 67(2):103+, February 1964.
- [2] R. Ivry and S.W. Keele. Timing functions of the cerebellum. *Journal of Cognitive Neuroscience*, 1(2):136–152, 1989.
- [3] E.R. Kandel, J.H. Schwartz, and T.M. Jessel. *Principles of Neural Science*. McGraw-Hill, New York, fourth edition, 2000.
- [4] M. Katayama and M. Kawato. Virtual trajectory and stiffness ellipse during multi-joint arm movement predicted by neural inverse models. *Biological Cybernetics*, 69:353–362, 1993.
- [5] S.W. Keele and R. Ivry. Does the cerebellum provide a common computation for diverse tasks? a timing hypothesis. *Annals of the New York Academy of Sciences*, 608:179–207, 1990.
- [6] M.U. Manto and M. Pandolfo. *The Cerebellum and its Disorders*. Cambridge University Press, Cambridge, UK, 2002.
- [7] S.G. Massaquoi. *Modeling the Function of the Cerebellum in Scheduled Liner Servo Control of Simple Horizontal Planar Arm Movements*. PhD dissertation, Massachusetts Institute of Technology, Department of Electrical Engineering and Computer Science, 1999.

- [8] S.G. Massaquoi and M. Hallet. Kinematics of initiating a two-joint arm movement in patients with cerebellar ataxia. *Canadian Journal of Neurological Sciences*, 23:3–14, 1996.
- [9] P. Trouillas, T. Takayanagi, M. Hallet, R.D. Currier, S.H. Subramony, K. Wessel, A. Breyer, H.C. Diener, S. Massaquoi, C.M. Gomer, P.Coutinho, M. Ben Hamida, G. Campanella, A. Filla, L. Schut, C. Timann, J. Honnorat, N. Nighoghossian, B. Manyam, and The Ataxia Neuropharmacology Committee of the World Federation of Neurology. Information capacity of discrete motor responses. *Journal of Neurological Sciences*, 145(2):205–211, February 1997.